


Theoretical modeling of the effective elastic constants of a sinusoidal anti-tetra-missing rib auxetic honeycomb

Miao Zhou¹, Xinxin Wu¹, Yunjian Cheng¹, and Yilin Zhu^{2,*} 

¹ School of Civil Engineering and Geomatics, Southwest Petroleum University, Chengdu 610500, PR China

² Center for Mechanics Plus under Extreme Environments, Faculty of Mechanical Engineering & Mechanics, Ningbo University, Ningbo 315211, PR China

Received: 30 November 2025 / Accepted: 21 January 2026

Abstract. Anti-tetra missing rib auxetic honeycombs represent a typical class of auxetic metamaterials exhibiting pronounced negative Poisson's ratio (NPR) effect. Conventional straight-ligament designs tend to incur stress concentrations at local nodes, whereas wavy configurations can effectively alleviate this issue. To elucidate the intrinsic relationship between microscopic geometric features and macroscopic mechanical properties, and to provide theoretical guidance for parameter-oriented structural design, this study develops an analytical model for the equivalent Poisson's ratio and elastic modulus of a sinusoidal anti-tetra-missing rib honeycomb (SATMRH) based on the energy method within the small-deformation framework. Finite element (FE) simulations are conducted to validate the analytical formulations. The results show that the proposed model agrees well with the numerical predictions and accurately captures the influence of geometric parameters on the macroscopic equivalent mechanical properties. Moreover, it is revealed that the structure maintains a nearly constant negative Poisson's ratio of approximately -0.65 , regardless of geometric variations, allowing stiffness tuning without sacrificing auxeticity. This work offers reliable theoretical support for the structural design and performance tailoring of ligament-based anti-chiral auxetic metamaterials.

Keywords: Negative Poisson's ratio / auxetic / metamaterials / honeycomb / chiral

1 Introduction

Auxetic metamaterials are a class of architected materials exhibiting a negative Poisson's ratio (NPR) [1,2]. When subjected to tensile loading, these materials expand laterally, displaying unconventional mechanical behavior that is difficult to achieve with conventional materials. Owing to their unique geometric tunability and multifunctional coupling characteristics, auxetic metamaterials have shown broad potential in energy absorption, flexible support, vibration control, smart regulation, and reconfigurable devices [3–13]. In recent years, honeycomb-shaped auxetic structures designed based on geometric configuration have attracted significant attention due to their lightweight, high strength, manufacturability, and parametric design capability [14–18]. Among these, optimizing the unit-cell geometry to tailor macroscopic performance has become a central research strategy.

Among various auxetic honeycombs, most adopt straight-ligament connections. While these structures are theoretically straightforward and exhibit clear deformation mechanisms, they often experience stress concentration at the junctions between nodes and connecting ligaments under loading, leading to local stiffness discontinuity and degradation of mechanical performance. To address this limitation, researchers have proposed curved-wall or curved-ligament honeycombs, which introduce geometric curvature to distribute stress, enhance compliance, and improve energy absorption. Replacing the straight ligaments with wavy ligaments, Zhu et al. [19,20] proposed wavy hexa-chiral and hexa-missing rib auxetic honeycombs with enhanced auxetic behavior in large deformations. Subsequently, Singh et al. [21] employed the wavy hexa-chiral configuration as the core layer of sandwich panels to enhance their resistance against blast loads. Liu and Zhang [22,23] proposed a series of soft-network auxetic honeycombs capable of achieving tailorable negative Poisson's ratios under large deformations, and conducted a theoretical investigation of their elastic constants. Zhang et al. [24] introduced an anti-tri-chiral auxetic topology featuring curved ligaments, demonstrating noticeable enhancements

* e-mail: zhuyilin@nbu.edu.cn; lin5210feng@163.com

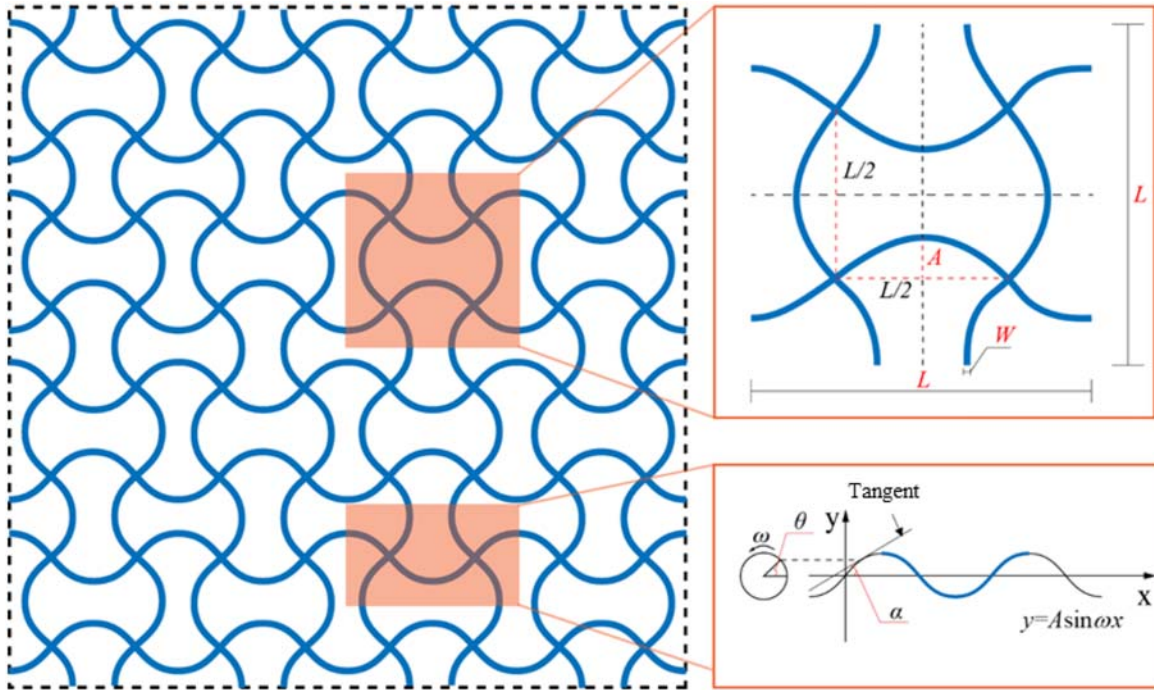


Fig. 1. Geometric description of the sinusoidal anti-tetra-missing rib honeycomb.

in its elastic response and capacity for energy dissipation. These studies highlight that introducing curvature is an effective strategy to improve mechanical properties of auxetic honeycombs and achieve tunable geometric functionality.

As a prominent representative of auxetic metamaterials, anti-tetra-chiral honeycombs exhibit unique geometric characteristics combining rotational and axial symmetry [25–29]. Their rotation core-ligament units undergo coordinated in-plane rotation under external loading, giving rise to a pronounced NPR performance. Depending on the form of the rotational core, anti-chiral configurations can be categorized into conventional anti-tetra-chiral structures, which employ circular rings, and missing rib anti-tetra-chiral structures (usually shorted as anti-tetra-missing rib structures), which use supporting frames as the central element. To further enhance the local mechanical response, researchers have incorporated wavy ligament designs into anti-tetra-chiral honeycombs. Introducing an effective and straightforward design-optimization framework, Wang et al. [30] developed both anti-tetra-chiral and anti-tetra-missing-rib lattices under prescribed stiffness constraints, enabling the realization of tailored effective mechanical properties. Zhang et al. [31] and Zhu et al. [32] further extended this line of research by developing inter-locking modular discrete structures based on the wavy anti-tetra-missing-rib configuration, and systematically investigated its crashworthiness performance. However, interestingly, investigations into the effective elastic properties of wavy anti-tetra-chiral structures are still lacking, limiting their practical design optimization and multifunctional applications.

Motivated by this, the present study investigates a sinusoidal anti-tetra-missing rib honeycomb (SATMRH). Within the small-deformation assumption, an analytical model for its equivalent elastic modulus and Poisson’s ratio is developed based on the energy method, and validated through FE simulations. The effects of geometric parameters, including wavelength, amplitude, and ligament thickness, on the equivalent elastic constants are systematically analyzed, revealing the modulation mechanism of macroscopic mechanical properties by the sine-shaped wavy anti-tetra-missing rib honeycomb.

2 Geometric description

The geometry of the SATMRH is depicted in Figure 1. The unit-cell of the structure consists of four interlaced sinusoidal ligaments, with an equation of

$$y = A \cdot \sin(\omega \cdot x), \text{ with } \omega = 2\pi/L, \quad (1)$$

where L , A and ω are the wavelength, amplitude and angular frequency of the sinusoidal ligaments, respectively. It is also indicated in Figure 1 that the structure can be fully described by three geometric parameters, i.e., the wavelength L (which also equals to the edge length of the unit-cell), amplitude A , thickness W of the ligaments. Noted that all the length parameters are measured along the neutral axis.

In addition, the structure investigated in this paper is a two-dimensional configuration, with its out-of-plane thickness normalized to unity.

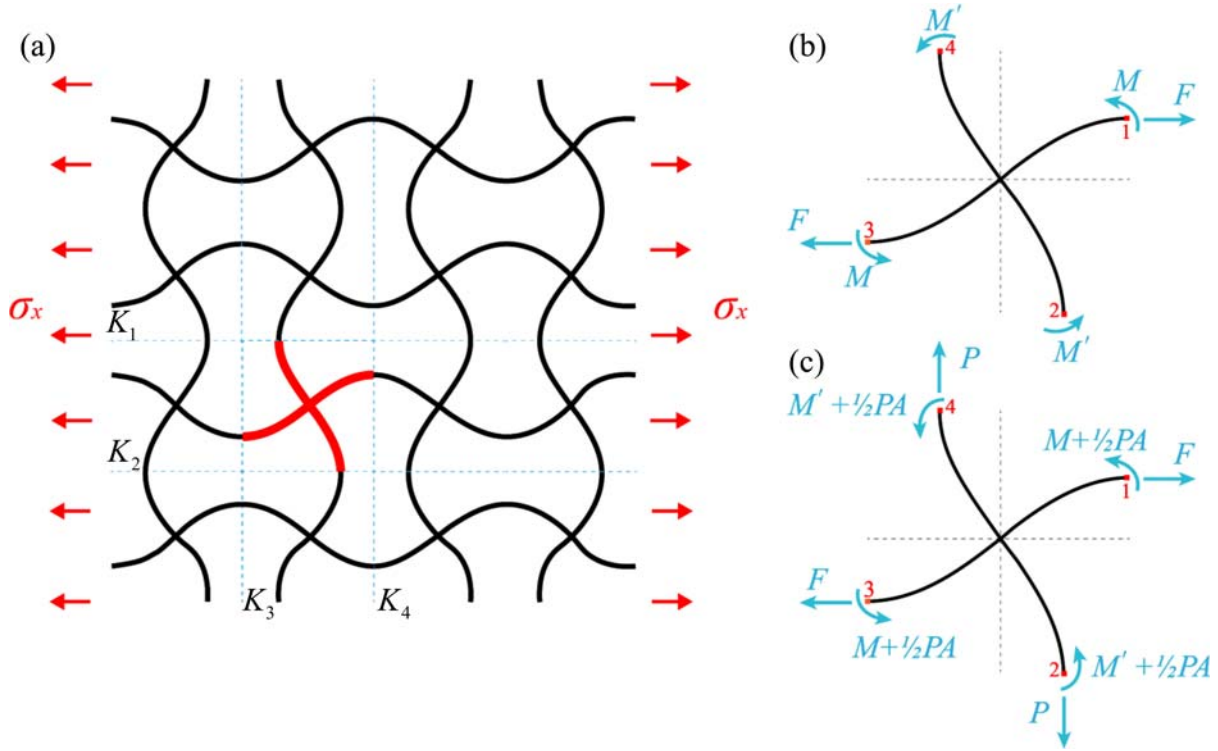


Fig. 2. (a). Schematic diagram of the SATMRH under uniaxial load; (b) free-body diagram of a smallest repeated unit (SRU), defined by symmetric cut-lines through the sinusoidal ligaments to ensure identical boundary forces and moments at corresponding cut points; (c) free-body diagram of a SRU incorporating the virtual force.

Moreover, for clarity and consistency, a baseline set of geometric parameters is adopted in the subsequent analyses, specified as $L : A : t = 20 : 3 : 0.5$ (units: mm).

3 Theoretical modelling

In this section, an energy-based approach (referring to Mousanezhad et al. [33]) is employed to derive theoretical expressions for the elastic constants of the SATMRH within the framework of linear infinitesimal elasticity. Noted that the SATMRH exhibits anisotropy, resulting in mechanical properties that vary with the loading direction. For the purpose of theoretical analysis, attention is restricted to a single loading direction (the horizontal direction, as illustrated in Fig. 2) to simplify the derivations.

Typically, we can analyze the effective elastic modulus and Poisson's ratio of a honeycomb by applying a far-field uniaxial tensile stress σ_x in the horizontal direction, as shown in Figure 2a. Figure 2b further provides a detailed free-body diagram (FBD) of the smallest repeating unit (SRU), which is defined by cutting lines $K_1 - K_4$. In this figure, the numbers “1”, “2”, “3”, and “4” indicate the external cut points of the sinusoidal ligaments. The following provides a further description. Owing to the two-fold rotational symmetry of the geometry and applied loads, corresponding external cut points in Figure 2b experience identical forces and moments. Furthermore, due to the axial symmetry of the structure and loading with respect to the cut lines as shown in Figure 2a, points “2” and “4” are free of forces in the

horizontal direction. Similarly, points “1” and “3” are free of forces in the vertical direction. Consequently, under the applied far-field stress σ_x , the forces and moments acting on the SRU are illustrated in detail in Figure 2b, where M and M' represent two unknown moments, and F is expressed as a function of the applied stress

$$F = \sigma_x L. \quad (2)$$

Considering the moment equilibrium in the out-of-plane direction yields

$$M + M' - FA = 0. \quad (3)$$

By accounting for both membrane and bending energies, the strain energy stored in the SRU is given by

$$\begin{aligned}
 U = & 2 \int_0^{\pi} \frac{1}{2} \frac{(F \cos \alpha)^2}{2E_s S} \cdot \sqrt{(A \cdot \cos \theta)^2 + \left(\frac{1}{\omega}\right)^2} d\theta \\
 & + 2 \int_0^{\pi} \frac{1}{2} \frac{[M - FA(1 - \sin \theta)]^2}{2E_s I} \cdot \sqrt{(A \cdot \cos \theta)^2 + \left(\frac{1}{\omega}\right)^2} d\theta \\
 & + 2 \int_0^{\pi} \frac{1}{2} \frac{(FA - M)^2}{2E_s I} \cdot \sqrt{(A \cdot \cos \theta)^2 + \left(\frac{1}{\omega}\right)^2} d\theta. \quad (4)
 \end{aligned}$$

The first term represents the membrane energy induced by the force F , while the latter two terms correspond to the bending energy contributions arising from the force F and

the moment M , respectively. Moreover, S and I are the cross-sectional area and moment of inertia of the ligament, respectively (for a rectangular cross-section with unit thickness, $S = t$ and $I = W^3/12$) and E_s denote the elastic modulus of the base material. In addition, α denotes the angle between the tangent to a point on the sinusoidal ligament and the x -axis, as illustrated in Figure 1. Accordingly, α is expressed as

$$\alpha = \arctan\left(A \cdot \frac{2\pi}{l} \cdot \cos\theta\right). \quad (5)$$

Applying Castigliano's theorem, a geometric condition is required to ensure that all corresponding outer ligaments in the SRU remain parallel under deformation. We hence have a constraint condition as

$$\partial U / \partial M = 0. \quad (6)$$

Substituting the strain energy from equation (4) into this constraint condition, we have

$$M = \eta FA, \quad (7)$$

with

$$\eta = \frac{\int_0^{\frac{\pi}{2}} \left(1 - \frac{\sin\theta}{2}\right) \cdot \sqrt{(A \cdot \cos\theta)^2 + \left(\frac{1}{\omega}\right)^2} d\theta}{\int_0^{\frac{\pi}{2}} \sqrt{(A \cdot \cos\theta)^2 + \left(\frac{1}{\omega}\right)^2} d\theta}. \quad (8)$$

In view of equations (3), (4), and (7), the strain energy of a SRU is finally rewritten as

$$U = \frac{F^2 \pi}{2E_s S \omega} + \frac{F^2 A^2}{E_s I} \int_0^{\frac{\pi}{2}} (\eta - 1 + \sin\theta)^2 \cdot \sqrt{(A \cdot \cos\theta)^2 + \left(\frac{1}{\omega}\right)^2} d\theta + \frac{F^2 A^2}{E_s I} \int_0^{\frac{\pi}{2}} (1 - \eta)^2 \cdot \sqrt{(A \cdot \cos\theta)^2 + \left(\frac{1}{\omega}\right)^2} d\theta. \quad (9)$$

Further according to Castigliano's second theorem, i.e., $\frac{\partial U}{\partial F} = 0$, the total displacement at points "1" and "3" in the horizontal direction (denoted as δ_x) is given by

$$\delta_x = \frac{F \pi}{2E_s S \omega} + \frac{2FA^2}{E_s I} \int_0^{\frac{\pi}{2}} (\eta - 1 + \sin\theta)^2 \cdot \sqrt{(A \cdot \cos\theta)^2 + \left(\frac{1}{\omega}\right)^2} d\theta + \frac{2FA^2}{E_s I} \int_0^{\frac{\pi}{2}} (1 - \eta)^2 \cdot \sqrt{(A \cdot \cos\theta)^2 + \left(\frac{1}{\omega}\right)^2} d\theta. \quad (10)$$

The effective elastic modulus (denoted as \bar{Y}) of the structure, normalized by the base material's elastic modulus E_s , is then defined as

$$\bar{Y} = \frac{\sigma_x L}{\delta_x E_s} = \frac{1}{\frac{\pi}{2S\omega} + \frac{2A^2}{I} \int_0^{\frac{\pi}{2}} (\eta - 1 + \sin\theta)^2 \cdot \sqrt{(A \cdot \cos\theta)^2 + \left(\frac{1}{\omega}\right)^2} d\theta + \frac{2A^2}{I} \int_0^{\frac{\pi}{2}} (1 - \eta)^2 \cdot \sqrt{(A \cdot \cos\theta)^2 + \left(\frac{1}{\omega}\right)^2} d\theta}. \quad (11)$$

Next, to determine the effective Poisson's ratio (denoted as $\bar{\nu}$), a pair of vertical virtual forces acting on the cut points of the SRU is considered, as illustrated in Figure 2c. Two virtual forces of magnitude P are applied at points "2" and "4". It should be noted that the overall equilibrium of the structure must still be maintained after applying the virtual forces, so a bending moment of $1/(4PA)$ is applied at each node. The strain energy of the SRU can then be modified as

$$U = 2 \int_0^{\frac{\pi}{2}} \frac{(F \cos\alpha)^2}{2E_s S} \cdot \sqrt{(A \cdot \cos\theta)^2 + \left(\frac{1}{\omega}\right)^2} d\theta + 2 \int_0^{\frac{\pi}{2}} \frac{(P \cos\alpha)^2}{2E_s S} \cdot \sqrt{(A \cdot \cos\theta)^2 + \left(\frac{1}{\omega}\right)^2} d\theta + 2 \int_0^{\frac{\pi}{2}} \frac{\left[M - FA(1 - \sin\theta) + \frac{1}{2}PA\right]^2}{2E_s I} \cdot \sqrt{(A \cdot \cos\theta)^2 + \left(\frac{1}{\omega}\right)^2} d\theta + 2 \int_0^{\frac{\pi}{2}} \frac{\left[FA - M + \frac{1}{2}PA - PA(1 - \sin\theta)\right]^2}{2E_s I} \cdot \sqrt{(A \cdot \cos\theta)^2 + \left(\frac{1}{\omega}\right)^2} d\theta. \quad (12)$$

The first two terms represent the membrane energy, while the latter two terms correspond to the bending energy, respectively.

Applying Castigliano's theorem again, the displacement of point "4" relative to point "2" in the vertical direction is obtained as

$$\delta_y = \frac{\partial U}{\partial P} \Big|_{P=0} = \frac{F^2 A^2}{E_s I} \int_0^{\frac{\pi}{2}} [\eta - 1 + \sin\theta]^2 \cdot \sqrt{(A \cdot \cos\theta)^2 + \left(\frac{1}{\omega}\right)^2} d\theta + \frac{F^2 A^2}{E_s I} \int_0^{\frac{\pi}{2}} (1 - \eta) \cdot \left(\frac{1}{2} + \sin\theta\right) \cdot \sqrt{(A \cdot \cos\theta)^2 + \left(\frac{1}{\omega}\right)^2} d\theta. \quad (13)$$

In view of equations (10) and (13), the effective Poisson's ratio ν of the SATMRH is derived as

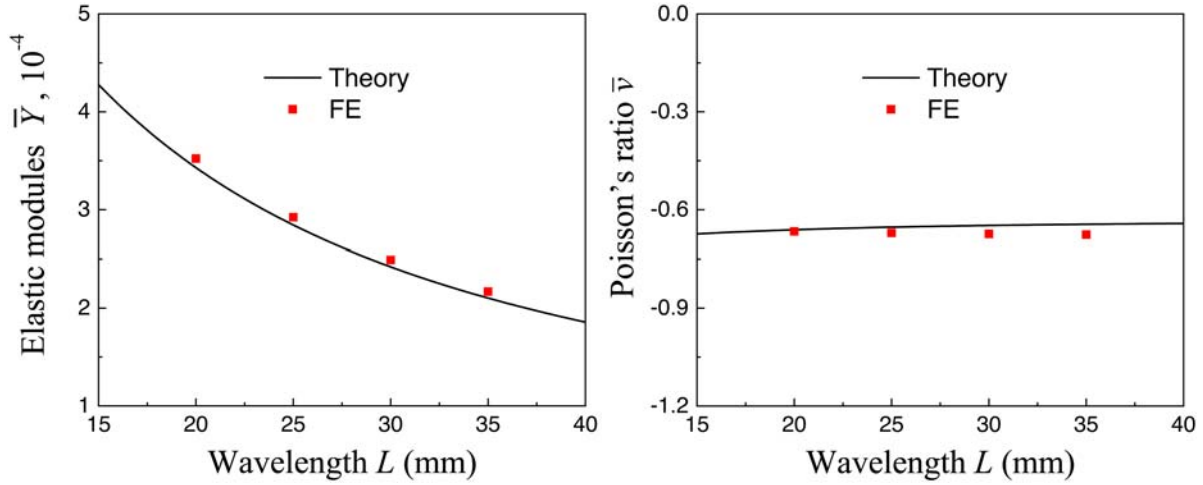


Fig. 3. Theoretical (lines) and FE (symbols) results of the effective elastic constants of the SATMRH over a range of the wavelength of the ligament ($A=3$; $t=0.5$). It is observed that the effective Poisson's ratio remains nearly constant across the investigated range of L .

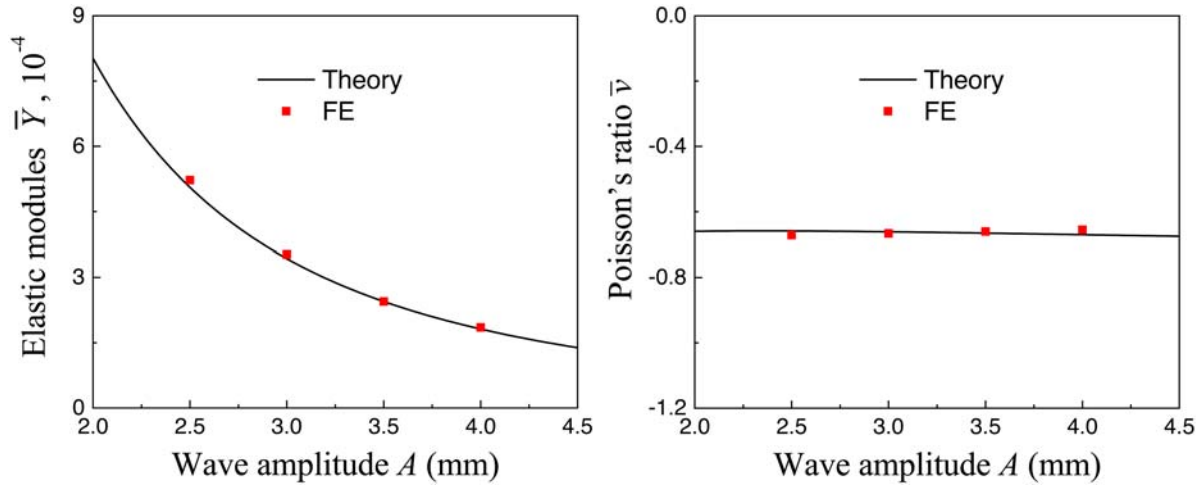


Fig. 4. Theoretical (lines) and FE (symbols) results of the effective elastic constants of the SATMRH over a range of the wave amplitude of the ligament ($L=20$; $t=0.5$). It is observed that the effective Poisson's ratio remains nearly constant across the investigated range of A .

$$\begin{aligned} \bar{\nu} &= -\frac{\delta_y F^2 A^2}{\delta_x E_s I} \int_0^{\frac{\pi}{2}} [\eta - 1 + \sin\theta]^2 \cdot \sqrt{(A \cdot \cos\theta)^2 + \left(\frac{1}{\omega}\right)^2} d\theta \\ &= -\frac{\frac{F^2 A^2}{E_s I} \int_0^{\frac{\pi}{2}} (1 - \eta) \cdot \left(\frac{1}{2} + \sin\theta\right) \cdot \sqrt{(A \cdot \cos\theta)^2 + \left(\frac{1}{\omega}\right)^2} d\theta}{\frac{\pi^2 t^2}{12} \frac{1}{\sqrt{A^2 \omega^2 + 1}} + 2\pi a^2 \left(\frac{\pi}{4} - \frac{1}{\pi}\right)}. \end{aligned} \quad (14)$$

4 Validations and discussions

In this section, FE simulations are conducted to substantiate the theoretical expressions derived in Section 3, and to further elucidate the dependence of the effective elastic constants on the relevant geometric parameters.

The FE analyses are carried out in ABAQUS using four-node bilinear quadrilateral elements under plane-strain conditions (CPS4). Based on a preliminary mesh-refinement study, an element length of $0.25W$ is adopted to ensure sufficient accuracy. As the theoretical formulations were established within the small strain regime, geometric nonlinearity is omitted in the present simulations. For the base material, the mechanical properties of VeroBlue RGD840 are adopted, with a Young's modulus of 2 GPa and a Poisson's ratio of 0.35 [34, 35]. Moreover, to minimize boundary effects, computational homogenization is performed on a unit-cell subject to periodic boundary conditions (PBCs), referring to Zhu et al. [19, 20].

Figures 3–5 illustrate how the three key geometric parameters (L , A , and t) influence the theoretically predicted effective elastic constants of the SATMRH, together with their validation through FE simulations. Noted that for each geometric parameter, its effect is analyzed while the other geometric parameters are kept

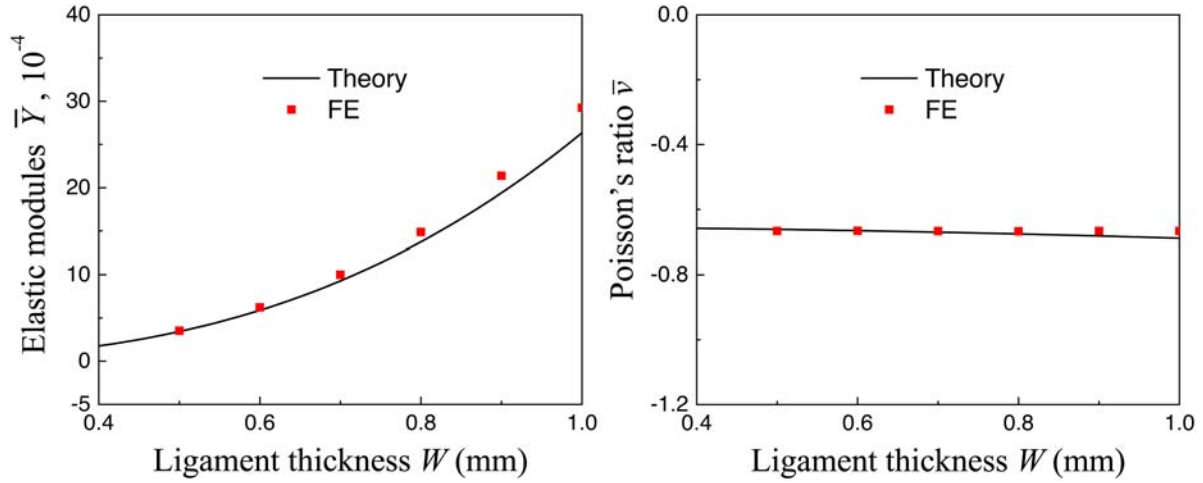


Fig. 5. Theoretical (lines) and FE (symbols) results of the effective elastic constants of the SATMRH over a range of the thickness of the ligament ($L=20$; $A=3$). It is observed that the effective Poisson's ratio remains nearly constant across the investigated range of t .

Table 1. Theoretical and FE results of the effective elastic constants for different wavelengths L .

| L | Elastic modulus $Y, 10^{-4}$ | | | Poisson's ratio $\bar{\nu}$ | | |
|-----|------------------------------|--------|-------|-----------------------------|--------|-------|
| | FE | Theory | Error | FE | Theory | Error |
| 20 | 3.52 | 3.43 | 2.65% | -0.666 | -0.662 | 0.74% |
| 25 | 2.92 | 2.84 | 2.70% | -0.671 | -0.654 | 2.65% |
| 30 | 2.49 | 2.42 | 2.82% | -0.674 | -0.648 | 3.86% |
| 35 | 2.17 | 2.10 | 3.01% | -0.676 | -0.645 | 4.68% |

Table 2. Theoretical and FE results of the effective elastic constants for different wave amplitudes A .

| A | Elastic modulus $Y, 10^{-4}$ | | | Poisson's ratio $\bar{\nu}$ | | |
|-----|------------------------------|--------|-------|-----------------------------|--------|-------|
| | FE | Theory | Error | FE | Theory | Error |
| 2.5 | 5.22 | 5.06 | 3.20% | -0.672 | -0.659 | 1.89% |
| 3 | 3.52 | 3.43 | 2.65% | -0.666 | -0.662 | 0.74% |
| 3.5 | 2.50 | 2.45 | 2.30% | -0.661 | -0.666 | 0.74% |
| 4 | 1.85 | 1.81 | 2.05% | -0.655 | -0.67 | 2.32% |

Table 3. Theoretical and FE results of the effective elastic constants for different thickness t .

| t | Elastic modulus $Y, 10^{-4}$ | | | Poisson's ratio $\bar{\nu}$ | | |
|-----|------------------------------|--------|--------|-----------------------------|--------|-------|
| | FE | Theory | Error | FE | Theory | Error |
| 0.5 | 3.52 | 3.43 | 2.65% | -0.666 | -0.662 | 0.74% |
| 0.6 | 6.21 | 5.89 | 5.22% | -0.666 | -0.666 | 0.04% |
| 0.7 | 9.99 | 9.29 | 7.01% | -0.667 | -0.670 | 0.50% |
| 0.8 | 14.9 | 14.0 | 6.04% | -0.668 | -0.676 | 1.22% |
| 0.9 | 21.4 | 19.0 | 11.22% | -0.667 | -0.682 | 2.26% |
| 1 | 29.2 | 26.0 | 10.96% | -0.667 | -0.689 | 3.33% |

constant. As shown in the figures, the FE results exhibit excellent agreement with the theoretical predictions. Tables 1–3 further summarize the discrepancies between

the FE simulated and theoretical results, with the maximum relative error remaining within 5%, thereby confirming the reliability of the proposed model.

As further illustrated in [Figures 3–5](#), variations in the geometric dimensions have almost no influence on the Poisson's ratio of the structure. Across all configurations, the structure consistently maintains a robust negative Poisson's ratio of approximately -0.65 . This indicates a desirable decoupling between stiffness tuning and auxetic behavior, demonstrating that the structural stiffness can be adjusted without compromising its auxeticity, which is highly advantageous for practical engineering applications.

In addition, the influence of each geometric parameter on the effective elastic modulus can be further clarified. The wavelength L is negatively correlated with the elastic modulus, since increasing L reduces the relative density of the structure, thereby lowering its stiffness. Similarly, the amplitude A is also negatively correlated with the elastic modulus, because a larger amplitude increases the flexibility of the ligaments, which clearly reduces the overall stiffness. In contrast, the thickness t exhibits a positive correlation with the elastic modulus, consistent with observations in other auxetic honeycomb structures.

Noted that the theoretical formulation in this work is developed within the framework of linear elasticity and small deformations, which is appropriate for evaluating the initial elastic response and effective elastic constants of the SATMRH. For moderate or large deformation regimes, geometric nonlinearity, ligament rotation, and potential contact effects may become significant, and the current analytical model may no longer be directly applicable. In such cases, nonlinear FE simulations and extended theoretical formulations would be required.

Nevertheless, despite the limitation associated with the small-deformation assumption, the proposed analytical model offers a highly efficient and physically transparent tool for rapid evaluation of effective elastic constants. Once the geometric parameters are specified, the analytical formulation enables instant predictions without the need for meshing, boundary-condition implementation, or iterative numerical solving. In contrast, FE-based homogenization generally requires repeated simulations, which can be computationally expensive when exploring multi-dimensional design spaces.

As a result, the proposed model is particularly advantageous for preliminary design, rapid parametric studies, and geometry optimization, while FE simulations remain essential for nonlinear and large-deformation analyses.

5 Conclusions

This study presents a comprehensive analytical framework for evaluating the equivalent mechanical properties of a sinusoidal anti-tetra missing rib honeycomb (SATMRH). The proposed model shows excellent agreement with FE simulations, confirming its accuracy and applicability. The results clarify the role of key geometric parameters in

tailoring structural stiffness, while demonstrating that the negative Poisson's ratio remains nearly constant at approximately -0.65 , irrespective of geometric variations. The key findings of this study can be summarized as follows:

(1) Validated analytical model

An energy-based analytical formulation was developed for predicting the effective elastic modulus and Poisson's ratio, and its accuracy was verified through FE simulations.

(2) Decoupling of stiffness and auxeticity

Geometric parameters significantly influence the effective stiffness, yet the structure consistently maintains a stable NPR of about -0.65 , enabling stiffness tuning without sacrificing auxetic behavior.

These findings provide solid theoretical support for the design optimization and performance customization of ligament-based anti-tetra-chiral auxetic metamaterials.

Specially, from an application-oriented perspective, the decoupled tunability between auxetic behavior and structural stiffness demonstrated in this work provides notable advantages for engineering design. The ability to maintain a stable negative Poisson's ratio while independently tailoring stiffness through geometric parameters makes the proposed SATMRH particularly suitable for applications such as impact mitigation and energy absorption, flexible supports and vibration isolation, as well as lightweight protective and adaptive structures. In these scenarios, geometry-based stiffness regulation can be achieved without compromising the intrinsic auxetic mechanism, offering enhanced design flexibility for multi-functional structural systems.

Acknowledgments

The numerical calculations in this paper have been done on the supercomputing system in the High Performance Computing Center of Southwest Petroleum University.

Funding

The financial support from the National Natural Science Foundation of China (12372143) is gratefully acknowledged.

Conflicts of interest

The authors declare that they have no known competing financial interests or personal relationships that could have appeared to influence the work reported in this paper.

Data availability statement

The data that support the findings of this study are available from the corresponding authors upon reasonable request.

Author contribution statement

Miao Zhou: Conceptualization, Formal analysis, Numerical simulation, Writing-original draft. Xinxin Wu: Methodology, Formal analysis, Validation. Yunjian Cheng: Supervision, Writing-review & editing. Yilin Zhu: Conceptualization, Supervision, Funding acquisition, Writing-review & editing.

References

1. J. Liu, D. Yan, W. Pang, Y. Zhang, Design, fabrication and applications of soft network materials, *Mater. Today* **49**, 324 (2021)
2. P. Sun, W. Yang, Y. Zhang, B. Zhang, Z. Fan, L. Li, Enhanced tensile properties of 3D printed soft-hard composites due to Poisson's ratio mismatch: Experimental and numerical study, *Composites Part B: Eng.* **299**, 112413 (2025)
3. S. Duan, L. Xi, W. Wen, D. Fang, A novel design method for 3D positive and negative Poisson's ratio material based on tension-twist coupling effects, *Composite Structures* **236**, 111899 (2020)
4. X.Y. Zhang, X.Y. Wang, X. Ren, Y.M. Xie, Y. Wu, Y.Y. Zhou, S.L. Wang, C.Z. Han, A novel type of tubular structure with auxeticity both in radial direction and wall thickness, *Thin-Walled Struc.* **163**, 107758 (2021)
5. X.Y. Zhang, X. Ren, X.Y. Wang, Y. Zhang, Y.M. Xie, A novel combined auxetic tubular structure with enhanced tunable stiffness, *Composites Part B: Eng.* **226**, 109303 (2021)
6. K.P. Logakannan, V. Ramachandran, J. Rengaswamy, D. Ruan, Stiffened star-shaped auxetic structure with tri-directional symmetry, *Composite Struc.* **279**, 114773 (2021)
7. Y. Zhang, X. Ren, X.Y. Zhang, T.T. Huang, L. Sun, Y.M. Xie, A novel buckling-restrained brace with auxetic perforated core: Experimental and numerical studies, *Eng. Struc.* **249**, 113223 (2021)
8. M. Balan, J. Mertens, M.R. Bahubalendruni, Auxetic Mechanical Metamaterials and their Futuristic Developments: A state-of-art Review, *Mater. Today Commun.* **35**, 105285 (2022)
9. R.A. Gomes, L.A. de Oliveira, M.B. Francisco, G.F. Gomes, Tubular auxetic structures: a review, *Thin-Walled Struc.* **188**, 110850 (2023)
10. X. Hou, V.V. Silberschmidt, *Metamaterials with Negative Poisson's Ratio: A Review of Mechanical Properties and Deformation Mechanisms* (Springer International Publishing, Berlin, 2015)
11. Z. Li, Y. Zhu, K. Yang, Modular metamaterials with strong auxeticity, tunability and crashworthiness, *Int. J. Solids Struc.* **321**, 113577 (2025)
12. C. Zhang, F. Lu, T. Wei, H. Wang, F. Liu, Y. Zhu, Windmill-shaped metamaterials achieving negative thermal expansion, *Eng. Struc.* **336**, 120488 (2025)
13. T. Wei, F. Lu, C. Zhang, Y. Huang, X. Rui, Y. Zhu, Energy absorption of 3D assembled auxetic meta-structure with compression-twisting effect, *Structures* **73**, 108482 (2025)
14. J. Zhang, Y. Xie, Z. Li, G. Ye, C. Zhang, T. Wang, L. Wang, Comparison of out-of-plane compression performance of cellular structures with different configuration: Hexagon, re-entrant, chirality, *Structures* **73**, 108396 (2025)
15. A. Gupta, S. Sharma, R.R. Madke, R. Chowdhury, In-plane mechanical behavior of tri-chiral and anti-trichiral auxetic cellular structures, *Int. J. Mech. Sci.* **289**, 110054 (2025)
16. W. Zhang, Z. Yan, J. Zhang, H. Wang, F. Han, P. Jiang, T. Wu, Q. Qin, On in-plane crushing behavior of an improved double-arrow auxetic metamaterial with two-step deformation mode, *Eng. Struc.* **303**, 117482 (2024)
17. R. Zhao, B. Yuan, D. Zhou, Z. Li, M. Zhao, Y. Tao, On the out-of-plane crashworthiness of incorporating hierarchy and gradient into hexagonal honeycomb, *Mech. Adv. Materi. Struc.* **31**, 5927 (2024)
18. Y. Dong, K. Chen, H. Liu, J. Li, Z. Liang, Q. Kan, Adjustable mechanical performances of 4D-printed shape memory lattice structures, *Composite Struc.* **334**, 117971 (2024)
19. Y. Zhu, S. Jiang, L.H. Poh, Y. Shao, Q. Wang, Enhanced hexa-missing rib auxetics for achieving targeted constant NPR and in-plane isotropy at finite deformation, *Smart Mater. Struc.* **29**, 045030 (2020)
20. Y. Zhu, Z.-P. Wang, L.H. Poh, Auxetic hexachiral structures with wavy ligaments for large elasto-plastic deformation, *Smart Mater. Struc.* **27**, 055001 (2018)
21. S.K. Singh, B. Vengatachalam, L.H. Poh, Sandwich panels with wavy hexachiral core layer against blast loads, *Thin-Walled Struc.* **218**, 114022 (2025)
22. J. Liu, Y. Zhang, Soft network materials with isotropic negative Poisson's ratios over large strains, *Soft Matter* **14**, 693 (2018)
23. J. Liu, Y. Zhang, A mechanics model of soft network materials with periodic lattices of arbitrarily shaped filamentary microstructures for tunable Poisson's ratios, *J. Appl. Mech.* **85**, 051003 (2018)
24. E.T. Zhang, H. Liu, B.F. Ng, Novel arc-shaped ligaments to enhance energy absorption capabilities of re-entrant anti-trichiral structures, *Composites Part B: Eng.* **227**, 109366 (2021)
25. A. Alderson, K.L. Alderson, D. Attard, K.E. Evans, R. Gatt, J.N. Grima, W. Miller, N. Ravirala, C. Smith, K. Zied, Elastic constants of 3-, 4- and 6-connected chiral and anti-chiral honeycombs subject to uniaxial in-plane loading, *Composites Sci. Technol.* **70**, 1042 (2010)
26. A. Bacigalupo, M.L. De Bellis, Auxetic anti-tetrachiral materials: equivalent elastic properties and frequency band-gaps, *Composite Struc.* **131**, 530 (2015)
27. Y. Chen, F. Scarpa, Y. Liu, J. Leng, Elasticity of anti-tetrachiral anisotropic lattices, *Int. J. Solids Struc.* **50**, 996 (2013)
28. W. Wu, Y. Tao, Y. Xia, J. Chen, H. Lei, L. Sun, D. Fang, Mechanical properties of hierarchical anti-tetrachiral meta-structures, *Extreme Mech. Lett.* **16**, 18 (2017)
29. Y. Zhang, L.-H. Ma, H.-Q. Xu, W. Zhou, A novel anti-missing-rib lozenge lattice metamaterial with enhanced mechanical properties, *Mater. Today Commun.* **38**, 108151 (2024)

30. Z.-P. Wang, Y. Wang, L.H. Poh, Z. Liu, Integrated shape and size optimization of curved tetra-chiral and anti-tetra-chiral auxetics using isogeometric analysis, *Composite Struc.* **300**, 116094 (2022)
31. Y. Zhang, X. Ren, W. Jiang, D. Han, X.Y. Zhang, Y. Pan, Y. M. Xie, In-plane compressive properties of assembled auxetic chiral honeycomb composed of slotted wave plate, *Mater. Design* **221**, 110956 (2022)
32. Y. Zhu, X. Wu, X. Rui, D. Gan, Q. Wang, C. Zhang, On the design and in-plane crashworthiness of a novel extendable assembled auxetic honeycomb, *Thin-Walled Struc.* **211**, 113123 (2025)
33. D. Mousanezhad, B. Haghpanah, R. Ghosh, A.M. Hamouda, H. Nayeb-Hashemi, A. Vaziri, Elastic properties of chiral, anti-chiral, and hierarchical honeycombs: A simple energy-based approach, *Theor. Appl. Mech. Lett.* **6**, 81 (2016)
34. J. Liu, Y. Zhang, Soft network materials with isotropic negative Poisson's ratios over large strains, *Soft Matter* **14**, 1693 (2018)
35. J.W. Snyder, A. Palazotto, Finite Element Design and Modal Analysis of a Hexakis Icosahedron Frame for Use in a Vacuum Lighter-Than-Air Vehicle, *J. Eng. Mech.* **144**, 04018042 (2018)

Cite this article as: Miao Zhou, Xinxin Wu, Yunjian Cheng, Yilin Zhu, Theoretical modeling of the effective elastic constants of a sinusoidal anti-tetra-missing rib auxetic honeycomb, *EPJ Appl. Metamat.* **13**, 11 (2026), <https://doi.org/10.1051/epjam/2026001>